

AU-Scale Synchrotron Jets and Superluminal Ejecta in GRS 1915+105.

V. Dhawan

vdhawan@nrao.edu

National Radio Astronomy Observatory, Socorro, NM 87801 ¹

I. F. Mirabel

mirabel@discovery.saclay.cea.fr

CEA/DSM/DAPNIA/SAP, Centre d'Etudes de Saclay, F-91191 Gif-sur-Yvette, France &
Instituto de Astronomía y Física del Espacio, Buenos Aires, Argentina

and

L. F. Rodríguez

luisfr@astrosmo.unam.mx

Instituto de Astronomía, UNAM, Apdo. Postal 70-264, 04510, México, DF, México

Received _____; accepted _____

Submitted to Ap.J.

¹The NRAO is a facility of the National Science Foundation operated under cooperative agreement by Associated Universities, Inc.

ABSTRACT

Radio imaging of the microquasar GRS 1915+105 with the Very Long Baseline Array (VLBA) over a range of wavelengths (13, 3.6, 2.0 and 0.7 cm), in different states of the black hole binary, always resolves the nucleus as a compact jet of length $\sim 10\lambda_{\text{cm}}$ AU. The nucleus is best imaged at the shorter wavelengths, on scales of 2.5 - 7 AU (0.2 - 0.6 mas resolution). The brightness temperature of the core is $T_{\text{B}} \geq 10^9$ K, and its properties are better fit by a conically expanding synchrotron jet model, rather than a thermal jet. The nuclear jet varies in ~ 30 min during minor X-ray/radio outbursts, and re-establishes within ~ 18 hours of a major outburst, indicating the robustness of the X-ray/radio (or disk/jet) system to disruption.

At lower resolution (80-240 AU), more extended ejecta are imaged at ~ 500 AU separation from the stationary core. Time-lapse images clearly detect the superluminal motion of the ejecta in a few hours. The measured velocity is $1.5 \pm 0.1 c$ ($D/12$ kpc) for the approaching component, and is consistent with ballistic motion of the ejecta from 500 AU outwards, perhaps even since birth. The axis of the ejecta differs by $\leq 12^\circ$ clockwise from the axis of the AU-scale jet, measured in the same observation. Both axes are stable in time ($\pm 5^\circ$), the AU scale for two years, and the large scale for over four years. Astrometry over two years relative to an extragalactic reference locates the black hole to ± 1.5 mas, and its secular parallax due to Galactic rotation is 5.8 ± 1.5 mas yr $^{-1}$, consistent with a distance of 12 kpc. Finally, a limit of ≤ 100 km s $^{-1}$ is placed on its proper-motion with respect to its neighbourhood.

Some accreting black holes of stellar mass (e.g. Cyg X-1, 1E 1740-2942, GRS 1758-258, GX 339-4) and supermassive black holes at the centre of galaxies (e.g. Sgr A*) lack evidence of large flares and discrete transient ejecta,

but have compact radio cores with steady, flat-spectrum ‘plateau’ states, like GRS 1915+105. Until now GRS 1915+105 is the only system where both AU-scale steady jets and large-scale superluminal ejections have been unambiguously observed. Our observations suggest that the unresolved flat-spectrum radio cores of accreting black holes are compact quasi-continuous synchrotron jets.

Subject headings: Subject headings: radio continuum: stars — stars: individual: (GRS 1915+105) — X-rays: stars

1. Introduction

The X-ray transient GRS 1915+105, discovered in 1992 by the *Granat* satellite, (Castro-Tirado et al. 1994), is one of a few Galactic sources exhibiting superluminal radio ejecta (see Mirabel & Rodríguez (1999) for a review). This microquasar offers a nearby laboratory for the study of black hole accretion, and the associated phenomena of jet formation, collimation, and outflow. Since the characteristic evolution time is proportional to the mass of the central black hole (Rees, 1998; Sams et al. 1996), microquasars can reveal in minutes a richness of phenomena analogous to a $10^8 M_{\odot}$ quasar observed over centuries.

In this paper, we present radio images of the microquasar GRS 1915+105, made with the Very Long Baseline Array (VLBA, see Zensus, Diamond, & Napier (1995)), in two distinct states of the black hole binary, the **plateau** and **flare** states. The **plateau** state is characterized by a flat radio spectrum, compact size of a few AU, and flux density 10-100 mJy. The XTE (2-12 keV) soft X-rays are weak, and the BATSE (20-100 keV) emission is strong. In contrast, during the **flare** state, with rise-time ≤ 1 day, optically thin ejecta of up to 1 Jy at $\lambda 13$ cm ($S_{\nu} \propto \nu^{-0.6}$), are expelled to thousands of AU and fade over several days. The soft X-rays also flare and show extreme variability, while the hard

X-rays fade for a few days before recovering. Observations over a range of wavelengths (13 cm, 3.6 cm, 2 cm and 0.7 cm), distinguish the intrinsically elongated nucleus, of length $\sim 10\lambda_{\text{cm}}$ AU, from angular broadening due to scattering by the line-of-sight ionized interstellar medium in the Galactic plane.

GRS 1915+105 was also imaged in its distinct state of pronounced X-ray dips, that repeat on timescales ranging from ~ 12 -60 min, with the same repetition rate seen in the IR and radio pulses. The radio and X-ray variability of GRS 1915+105 showed early evidence for recurrent accretion and jet formation (Rodríguez & Mirabel 1999; Foster et al. 1996). There now exists a wealth of data from X-ray, IR and radio observations, offering clues to the coupled evolution of accretion disk, corona, and jet. On several occasions, the flux of thermal X-rays from the inner accretion disk has been observed to diminish, with simultaneous hardening of the power-law spectrum from relativistic electrons, followed by progressively delayed emission in the IR and radio, (Mirabel et al. 1998; Markwardt et al. 1999; Belloni et al. 1997b; Eikenberry et al. 1998; Pooley & Fender 1997; Fender et al. 1997, 1998). One scenario is to have the inner part of the accretion disk and corona accelerated to relativistic speeds, and ejected as synchrotron-emitting plasma. Alternatively, advective infall of the disk past the black hole horizon (Narayan et al. 1997), could account for the X-ray dips, but not for the IR and radio emission. A solution allowing simultaneous inflow and outflow is presented in the ‘ADIOS’ (Advection Dominated Inflow-Outflow Solution) model of Blandford & Begelman (1999), but mechanisms to produce the observed X-ray variability without ADAF (Advection Dominated Advection Flow) are discussed in Nayakshin et al. (1999). Though the mechanism is still debated, this particular source switches the jets on and off, presenting repeated but unpredictable opportunities to observe the ejecta evolve from scales of a few to thousands of AU.

2. VLBA Observations

Triggered by GBI ² daily monitoring, we have coordinated observations with X-ray and IR telescopes, followed the radio variations with the VLA (Mirabel et al. 1998), and imaged the radio emission at multiple wavelengths with the VLBA (this paper). Crucial capabilities of the VLBA were the dynamic scheduling in response to transients, and phase-referencing which permits astrometry and the detection of weak sources.

The VLBA observation epochs and parameters are presented in Table-1. Observations are possible in any of nine wavelength bands, with band changes requiring 20 s or less. Simultaneous data can be obtained from the 3.6 cm/13 cm receiver pair, by means of frequency-selective optics. The choice of band was made just before each observation, based on the most recent flux and spectral information. Observations at 2 cm and 7 mm are least affected by galactic electron scattering, and were used to observe the AU scales when the radio-to-IR spectrum was flat. During the steep-spectrum flares, we employed the 3.6 cm/13 cm pair to image large-scale ejecta. Other bands were observed for ~ 20 -40 mins in rotation. We employed the highest data recording rates, (256 or 128 Mb s⁻¹, subject to scheduling constraints), for maximum sensitivity in short time, since the source is known to be highly variable. Ultimately, our image quality is limited not by thermal noise, but by the restriction of instantaneous UV coverage to a maximum of 45 baselines (Fourier components) from 10 antennas.

EDITOR: PLACE TABLE 1 HERE.

All the VLBA observations (except 7 mm) were phase-referenced, i.e., the antennas

²The Green Bank Interferometer is a facility of the National Science Foundation operated by NRAO with support of the NASA High Energy Astrophysics programs.

alternated between the target and one of several extragalactic calibrators of known (sub-millarcsec) position. Cycle times of three minutes were adequately fast to follow tropospheric phase fluctuations at 2 cm and longer wavelengths. Thus the interferometer array was rendered coherent for many hours, and the resulting astrometric accuracy of ~ 1.5 mas allows us to discriminate between moving and fixed source components. In addition, with frequent amplitude calibration, we avoid blind self-calibration on the time-variable target.

We generated time-resolved images, with snap-shot intervals ranging from 5 to 60 mins, depending on the beam size. Self-calibration was used self-consistently, i.e. only over the snapshot interval. Snap-shots were averaged in the image plane and UV data were combined over longer intervals only if the snapshots were indistinguishable. In practice, there is little effect at lower resolutions from the moving ejecta - mainly a blurring of the moving component, and an increase in residual artifacts, since self-calibration does not work perfectly if the structure is varying. (See e.g., Fig. 2B, where the extension of the SW component away from the core has occurred during the ‘exposure time’ of 5.1 hr.)

For the high-resolution images (e.g. in Fig. 5), the problem of reliable imaging is more severe. In addition to snapshot imaging, a careful search for time-variable or moving structure was done by examining and model fitting to the closure phases over intervals as short as 5 mins. Simultaneous flux measurement (from the VLA or GBI, when available) was used to constrain the total flux while modelling the AU-scale structure. No evidence for rapidly moving or variable structures was found. We can rule out discrete, moving ejecta on AU scales - none of the snapshots or closure phases showed, e.g. double sources or differently oriented structures. We cannot at this time rule out fast-moving features with low contrast, that would be blurred out. The simulations can be used to place limits on the artifacts due to the technique, to be discussed in a future paper. We will continue to pursue

evidence for AU-scale motion in new data, as well as old data after further refinement in software to model moving, time-variable sources.

3. Images During Two Flares

These target-of-opportunity observations are subject to the constraints of weather, scheduling, and source variability. For clarity, we present individual images for two episodes of flare activity, and merge the discussion of the common elements thereafter.

3.1. 1997 October

The radio and X-ray behavior of GRS 1915+105 around this flare is summarized in Fig. 1. The AU-scale jet is imaged in the nucleus (Fig 2A) on 1997 October 23, six days before a major flare. Images on October 31, centered at MJD 50752.02, (Fig. 2B & C) show the central core with a bright component 47.5 ± 0.3 mas away on the SE (approaching) side. The core has a flux density of ~ 20 mJy with flat spectrum, while the SE ejected component has $S_\nu \propto \nu^{-0.5}$. The position of the SE component corresponds to a separation rate of 0.90 ± 0.05 mas hr $^{-1}$ in 53.3 ± 2.4 hrs since the estimated start of the flare at MJD=50749.8. A NW (receding) component is marginally detected, at 17.4 ± 0.3 mas separation, consistent with it being the counter-ejection, with velocity 0.33 ± 0.02 mas hr $^{-1}$ and flux density only $\sim 10\%$ of the SE component.

The time-lapse images, (Fig. 3), with interval of 2.5 hrs, show a separation change of the SE ejection from the core of 2.3 ± 0.2 mas, or 0.92 ± 0.08 mas hr $^{-1}$. Our start time for the flare is derived by extrapolating the slopes of the X-ray and radio data (see Fig. 1). With this start time the velocity derived from the position of the ejecta after 53.3 hours agrees with the velocity from the 2.5 hr time lapse images. Fender et al. (1999) assume a

considerably different start at 50750.5 for the same flare. However, their velocities for the ejecta, derived from images several days after the flare, at 500 to 5000 AU scales, agree with ours within the errors, and imply ballistic motion from a few to 1000's of AU, certainly beyond 500 AU.

EDITOR: PLACE FIGURE 1 HERE.

EDITOR: PLACE FIGURE 2 HERE.

EDITOR: PLACE FIGURE 3 HERE.

Astrometry (see Fig. 7) before and after the flare locates the nucleus within 1.5 mas of the position we have measured for over two years, after allowing for secular parallax. The 2 cm flux density varies with the 30 min period seen in XTE dips, starting at 50750.5 (Fender et al. 1999). We show that the variable radio emission is from the AU-scale jet, see Fig. 9; (see also Mirabel et al. (1998); Pooley & Fender (1997); Fender et al. (1997)). We conclude that the nuclear jet that we image has re-established itself within ~ 18 hrs of the start of a major outburst, if indeed it was disrupted at all. The position angle of the AU-scale jet in Fig. 2A is $157 \pm 2^\circ$ at 2 cm, whereas the large-scale ejecta show $133 \pm 3^\circ$ at 13 cm, in Fig. 2B; and $143 \pm 4^\circ$ at 3.6 cm in Fig. 2C.

3.2. 1998 April-May

The radio and X-ray behavior of GRS 1915+105 around this flare is summarized in Fig. 4. As in the 1997 October event, there is a jet in the nucleus during the plateau state,

(see Fig. 5D), two days before the flare which started on MJD \sim 50916. Figures 5E and 5F also show compact jets 2 days after the start of a second flare on MJD \sim 50932. The spectrum of the jet is essentially flat from 2 cm to 0.7 cm. After two intervening flares, on MJD 50935.5, the nucleus is still within 1.0 mas of the expected position, after allowing for secular parallax. The position angles of the AU-scale jet are as follows: D: $155\pm 2^\circ$, at 2 cm; E: $154\pm 4^\circ$ again at 2 cm; F: $145\pm 6^\circ$, at 0.7 cm for the overall structure, although the innermost contours are rotated to $168\pm 5^\circ$, perhaps indicating a bent jet.

The phase-referenced image at 2 cm (Fig. 6), heavily tapered to 100 AU beam size, shows the SE ejection at \sim 650 AU from the core. The counter-ejection was not detected, with flux $\leq 5.5\%$ of the approaching component. The separation from the core of the SE component corresponds to a motion of 57.5 ± 0.5 mas in 67 ± 7 hrs, or 0.87 ± 0.10 mas hr $^{-1}$. This is consistent with the velocity of 0.93 ± 0.07 mas hr $^{-1}$, seen in the red and blue snapshots in Fig. 6, which are 4.5 hrs apart. The position angle of the SE component is $148\pm 4^\circ$ from the core.

EDITOR: PLACE FIGURE 4 HERE.

EDITOR: PLACE FIGURE 5 HERE.

EDITOR: PLACE FIGURE 6 HERE.

4. Astrometry

Astrometry is vital to register moving components from one epoch to the next. The present astrometric accuracy is achieved with phase residuals to the VLBA correlator

model, and no special software. The correlator model used in these observations was in error by ~ 30 mas for Earth nutation, reduced by a factor of 0.1 due to the $\sim 5^\circ$ distance to the calibrator. We thus expect a maximum error in the absolute position determination of 3 mas for a given epoch. In fact, when we compare our positions for secondary calibrators in these observations to those obtained independently for the same calibrators in the same reference frame by USNO, we find agreement within 1.5 mas, (T.M. Eubanks, private communication). The effects of nutation error rate on proper motion are further reduced by the time-differencing, and are < 0.3 mas yr $^{-1}$. Our errors in the secular parallax are ~ 1.5 mas yr $^{-1}$, dominated by tropospheric ‘seeing’, i.e., residual phase errors from the calibrator. This can be seen in Fig. 7 as the short-term scatter of positions over a few hours on a given date.

EDITOR: PLACE FIGURE 7 HERE.

The J2000 position of the core is $19^h 15^m 11^s.54938 \pm 0.00007$, $10^\circ 56' 44'' .7585 \pm 0.001$, on 1998 May 02, in the ICRF reference frame (Ma, et al. 1998). The secular parallax is -5.4 ± 1 mas yr $^{-1}$ and -2.3 ± 1 mas yr $^{-1}$ in RA and Dec respectively. This level of astrometric accuracy, though it can be improved by further analysis, is adequate to demonstrate that:

(i) The identification of the stationary core and moving ejecta is unambiguous. We note that the 1997 October 31 data at 3.6 cm are shifted from the pre-flare position by ~ 2 mas, probably due to the complex and evolving structure during the flare. However, this error is not enough to cause mis-identification of core with ejecta separated by 47.5 mas.

(ii) GRS1915 shows the galactic rotation expected from an object about 12 kpc distant, (Dhawan et al. 2000), at the position $l = 45^\circ 37'$, $b = -0^\circ 22'$. We find a proper motion of 5.8 ± 1.5 mas yr $^{-1}$, which we ascribe to the secular parallax of the core, within errors of ± 75 km s $^{-1}$ in the plane of the Galaxy (all errors are $\pm 3\sigma$). A model-independent distance

may perhaps be determined in the future by measuring the annual trigonometric parallax of $\sim \pm 80 \mu\text{arcsec}$, using closer calibrator sources, as attempted in the case of Sgr A* (Reid et al. 1999).

(iii) The core is stationary on the sky to $\pm 1.5 \text{ mas}$ once the secular parallax is accounted for. The systematic drift perpendicular to the Galactic plane over two years is consistent with $0 \pm 50 \text{ km s}^{-1}$.

Combining errors parallel and perpendicular to the galactic plane, we can place an upper limit of $< 100 \text{ km s}^{-1}$ for the velocity of GRS 1915+105 on the sky. Note that velocity along the line of sight is unconstrained by these observations, but could become evident in the Doppler shift of periodic features, if any are detected in the future.

5. Scattering in the ISM Towards GRS 1915+105.

GRS 1915+105 lies near the galactic plane, along a line of sight tangential to a spiral arm and intercepting a large column of gas, both neutral and ionized. The high dispersion measure of distant pulsars in this direction (Taylor & Cordes 1993) leads us to expect considerable angular broadening due to the inhomogeneous ionized interstellar medium, as is indeed the case.

Observation over several octaves can separate the intrinsic structure from the scatter-broadening, as shown in Fig. 8, and short wavelengths (2 cm and 0.7 cm) were used to give an unscattered view into the nucleus where the jet originates. The minor axis size scales as λ^2 , and we measure a scattering size of $1.9 \pm 0.1 \text{ mas}$ at 3.6 cm, (135 mas at 30 cm = 1 GHz). Interestingly, the scattering seems to vary dramatically on scales of $\sim 50 \text{ pc}$, seen by comparing our result with the 8.4 mas at 30 cm, (measured by Kembell et al. (1988)) for the OH maser in OH45.47+0.13, which lies beyond the tangent point, as is

the case for GRS 1915+105, and only 10' away on the sky. A fraction of this increase by a factor of 16 in scattering could be due to a putative ionized circumstellar cocoon around the X-ray binary, as suggested by recent infrared spectroscopy with the VLT, (Martí et al. 2000).

EDITOR: PLACE FIGURE 8 HERE.

6. Two Distinct Radio Emission Phenomena?

We discuss in this section the evidence for two distinct radio emission states, described most simply as attached to, and detached from the nucleus. They correspond to:

- (a) A smooth, flat spectrum, continuous nuclear jet at AU scale, with quiescent or oscillating radio flux; and
- (b) Discrete ejecta, separating from the nucleus superluminally at $\geq 1.3 c$, during steep spectrum flares.

The major outbursts appear qualitatively different from the 30 min variations, and seem to have a different trigger. For **flares**, the onset of radio emission seems to correlate with the **rise** of 2-12 keV X-rays (see Figs. 1 & 4). On the other hand, the AU-scale (30 min) radio/IR oscillations are seen when deep XTE **dips** of ≤ 5000 counts are present. On the short timescale of 10's of minutes, isolated (single) events have not been observed to our knowledge - they are always part of a pulse-train, accompanied by X-ray dips. On the other hand, no periodicity or regularity has been observed in the timing of the large flares, which are always isolated events. More details of the two phenomena follow.

6.1. The AU-Scale Jet in the Nucleus

Our images are consistent with a conventional model of conical expanding jet, (Hjellming & Johnston (1988); Falcke & Biermann (1999), see also Sec.7) i.e., incoherent synchrotron emission in an optically thick region of size $\sim 10\lambda_{\text{cm}}$ AU, inclined at $\sim 66\text{-}70^\circ$ to the line of sight. The brightness temperature of the jet is $T_{\text{B}} \geq 10^9\text{K}$ at all wavelengths. ($T_{\text{B}}=10^9\text{K}$ at 0.7 cm, where the minor axis is marginally resolved because the scattering is least. At 2 cm and longer wavelengths, we measure the same brightness temperature, but it is a lower limit because the scattering size dominates the beam resolution, and the intrinsic width could be smaller.)

The images clearly identify the AU-scale jet with the **plateau** state and its quasi-periodic flux variations. The radio light curve of the jet is best described as a smoothed response, with time-constant of ~ 30 min, to the injection of relativistic plasma, presumably generated during the X-ray dips, (Figs. 9 & 10). The injection interval is variable, 12-60 mins have been observed on various occasions. The time delay between the shorter and longer radio wavelengths is also variable, from 4 min to ~ 30 min. Possible causes include changes in the size, expansion rate, or optical depth of the jet, or variable dynamics of accretion and jet formation. Variable orientation appears not to be a major contributing factor.

EDITOR: PLACE FIGURE 9 HERE.

EDITOR: PLACE FIGURE 10 HERE.

During a radio flare, one expectation might be that the radio core would fade as the inner accretion disk was ejected and/or swallowed. However, we find that the nuclear jet re-establishes itself within 18 hrs of the start of a major outburst, if it disappears at all.

The AU-scale structure is smooth, with little evidence for discrete, moving ejecta. This can be currently ascribed to the difficulty of Fourier synthesis imaging of moving, time-variable sources, rather than to a true lack of relativistic flow. A static structure is unlikely, given that we see superluminally moving ejecta on larger scales *during the same event*. A more likely explanation is a steady state with fast, continuous flow and adiabatic losses which cause the jet to fade rapidly with distance. The travel-time along the length of the jet ($\sim 10 \text{ AU hr}^{-1}$) at relativistic speed is comparable to the adiabatic loss timescale ($\sim 30 \text{ min}$) over which new IR/radio emission fades away after each X-ray injection event. Analogous compact jets may be found in Cygnus X-1 and Cygnus X-3, as suggested by Fender et al. (2000) from the flat radio-millimeter spectra of the cores in these X-ray binaries.

Good evidence exists that the synchrotron spectrum extends up to 2μ in the IR (Eikenberry et al. 1998; Mirabel et al. 1998; Fender et al. 1998). The IR light curves are quite similar to the radio, believed to be caused by rapid adiabatic expansion rather than synchrotron losses, as suggested by Fender et al. (1998) and Mirabel et al. (1998). Maximal internal energy (Falcke & Biermann 1999) implies expansion at $\sim 0.6 c$. The VLA measured expansion rate (Rodríguez et al. 1995) is about $0.2 c$ on large scales. On AU scales, we see an elongated structure with length about four times the width, which is consistent with relativistic flow along the major axis and lateral expansion at $0.2 c$.

Considering next the position angles of the AU-scale images, no significant time variations are seen. The AU-scale position angle is stable within $\sim 5^\circ$ for ~ 2 years. The 500 AU ejecta have the same P.A. for our two measurements in 1997 and 1998. The large ejection reported in Mirabel & Rodríguez (1994) was along $\sim 150^\circ$, about 7° CCW. We measure a rotation of about $12 \pm 5^\circ$ from the few-AU to the 500 AU scale, though both seem to be stable in time. This rotation of position angle with size scale appears real. We suspect

it could be due to opacity effects in a conical jet, since the high resolution is obtained at shorter wavelengths - however we do not have a clear explanation for it.

In summary, a synchrotron jet (see also Discussion) accounts in a unified, consistent way for the following phenomena:

- The flat radio spectrum and high brightness temperature.
- The elongation of the core along the axis of arcsecond-scale superluminal ejecta, ($\sim 155^\circ$).
- The peak emission is progressively delayed at longer wavelengths, as they emanate from further along the expanding jet;
- There is progressively less variation of the flux at longer wavelengths, due to convolution over a larger region;
- The decay time of flux variations is consistent with the travel time of relativistic plasma along the jet.

However, we must point out that the ratio of integrated flux density of approaching to receding parts of the continuous jet are only 1.15 ± 0.04 , 1.20 ± 0.05 , and 1.10 ± 0.08 , for the three images of Fig. 5A, B, C respectively. (Assuming we are seeing both sides of the jet; see the next paragraph for a possible exception). Assuming an inclination $\theta = 70^\circ$, a flat spectral index ($\alpha = 0$), and a continuous jet ($k = 2$), we obtain a mildly relativistic speed of $\beta_F = 0.1$ for the AU-scale jet, from the flux ratio (see, e.g., Bodo & Ghisellini (1995), eqn.4, for a stationary jet, with pattern speed $\beta_S = 0$, and bulk flow at speed β_F):

$$\left(\frac{S_{\text{approaching}}}{S_{\text{receding}}} \right) = \left(\frac{1 + \beta_F \cos\theta}{1 - \beta_F \cos\theta} \right)^{k-\alpha} \quad (1)$$

This result of 0.1c from the jet/counter-jet asymmetry is puzzling, in light of the expected relativistic flow in the jet model. We offer three possible explanations, none completely satisfactory:

Slow Mini-Jet? The jet/counter-jet ratio on AU scales is really due to slow jet velocity of 0.1c. This contradicts some of the data, and we do not favour it. First, the measured speed of 0.9c at 500 AU implies acceleration of ejecta from 0.1c to 0.9c between 20 AU and 500 AU, very far from the black hole ($>10^8 R_s$). This seems very unlikely. Secondly, as discussed above, the expansion speed of the synchrotron cloud must be fast, in at least one dimension, to account for the rapid fading of emission from adiabatic loss. (synchrotron radiative decay would take years, not 30 min as observed). The size and elongation of the jet, ~ 20 AU, implies the speed is $\sim c$, in at least one direction. For jet speed of 0.1 c, the isotropic expansion would dominate, so the AU-scale images would be circular, and endure for over 10 hrs.

Fast Mini-Jet? On the other hand,³ the brightness temperature of an optically thick synchrotron source should be about 10^{11} K, (predicted by the Falcke model as well) for a bulk Doppler factor ~ 1 , whereas we measure 10^9 K at 0.7 cm. If we assume a fast mini-jet, with bulk $\beta_F \geq 0.99$, then, because of the large inclination of 70° , the (approaching) doppler factor is ≤ 0.2 and the observed brightness temperature is reduced. This argues for a highly relativistic mini-jet on scales of few AU, that slows down as it reaches 1000 AU. Unfortunately, there is no observational evidence for deceleration, such as brightening due to hitting a density enhancement, at that radius. The jet/counter jet ratio would require explanation as in the next paragraph.

³We acknowledge discussion with Peter Goldreich.

Hidden Counter-Jet? We can postulate that the (receding) counter-jet is hidden by free-free absorption in the inclined disk, and only the approaching mini-jet is observed, with nearly symmetric brightness profile. This absorption geometry has been clearly demonstrated in 3C84, (Walker et al. 2000). In GRS 1915+105, the absorption must occur within 1000 AU of the core, because the counter-ejection is seen outside that radius, (Fender et al. 1999; Mirabel & Rodríguez 1994; Rodríguez & Mirabel 1999) We detect no counter-ejection at <500 AU in 1998 May 02 ($\tau > 1.5$ at 2 cm), and on 1997 October 31 there is a weak counter-ejection at a flux reduced from the expected beaming model, (Mirabel & Rodríguez 1994) indicating $\tau \sim 0.5$ at 3.6 cm, (sec.3.1 and 3.2). Different opacity for each ejection could be due to variable ionizing illumination from the disk, or variable mass-loss, for both of which ample evidence exists. Thus free-free opacity hiding the counter-jet on AU-scales, and hiding the counter-ejecta within a few 100 AU of the core, is consistent with the images. Assuming $\tau_{\text{free-free}} \sim 1$, $L \sim 100$ AU, we derive an electron density $n_e = 5 \cdot 10^5 \text{ cm}^{-3}$, emission measure $EM \sim 2 \cdot 10^8 \text{ cm}^{-6} \text{ pc}$, and column density $\sim 10^{21} \text{ cm}^{-2}$, for an electron temperature $T_e = 10^4 \text{ K}$.

Furthermore, we might explain both the enhanced scattering (Section-5) and the free-free opacity as signatures of the ionized envelope detected by Martí et al. (2000). However, the scattering is measured against the core, and the absorption is invoked against the counter jet, *not* the core, so special geometry is needed. We leave this as a speculation. The test would be to actually observe the counter jet and measure its spectrum which should be strongly rising with frequency, since the opacity is exponentially less at shorter wavelength, (Walker et al. 2000). Sensitive, technically difficult observations would be required at 0.7 cm or 0.3 cm.

6.2. The Ejecta at ~ 500 AU

Images during flares show rapidly decaying superluminal ejecta. Snapshots taken a few hours apart allow us to measure, for the approaching ejection, a velocity of $1.28 \pm 0.07 c$ ($D/10$ kpc) at 500 to 600 AU away from the nucleus, consistent with the velocity of Fender et al. (1999) at 5000 AU for the same event. This implies ballistic motion from 500 AU to 5000 AU. Phase-referencing clearly distinguishes the stationary core from the moving ejecta, unlike previous observations. Next, back-extrapolation of the position of the ejecta (over 2-3 days), using the velocity measured over a few hours, gives a position coincident with the core at the start time of the flares. Thus, on average, this is consistent with ballistic motion from the few-AU scale outwards. The lateral expansion rate of the ejecta is about 0.14 - $0.2c$, and is not well constrained in the VLBA images due to the lack of sensitivity to extended structure. The value of $0.2 c$ was measured in the VLA images on larger scales, (Rodríguez & Mirabel 1999).

7. Discussion

In this section we discuss a possible thermal origin for the emission, and decide in favor of a synchrotron jet. We also find good consistency between the synchrotron model of Falcke & Biermann (1999) and the disk instability model of Belloni et al. (1997a,b) for the source of the relativistic plasma in the baby jets. The large ejecta require ~ 10 times more mass, and may be qualitatively different from the AU-scale jets as well.

7.1. Thermal Jet

We rule out a thermal origin for the emission in favor of a synchrotron jet by the following argument. If we assume that the radio emission is due to free-free (thermal)

radiation from gas with an electron temperature of $\sim 10^{10}\text{K}$, and follow the formulation of Reynolds (1986) for the mass loss rate in a thermal jet, we roughly estimate

$$\left(\frac{\dot{M}}{M_{\odot} \text{ yr}^{-1}}\right) = 4 \times 10^{-4} \left(\frac{v}{10^4 \text{ km s}^{-1}}\right) \quad (2)$$

where v is the velocity of the outflowing gas. If this velocity were of the order of the speed of sound in a gas of 10^{10}K , $v=10^4 \text{ km s}^{-1}$, then a mass loss rate of $\sim 4 \times 10^{-4} M_{\odot} \text{ yr}^{-1}$, a mechanical power of $3 \times 10^6 L_{\odot}$, and an X-ray luminosity of the jet of $\sim 10^7 L_{\odot}$ are derived. These powers are similar to the Eddington luminosity of a $\sim 100 M_{\odot}$ black hole, and appear excessive for what is known of GRS 1915+105.

Finally, the QPO's observed in the radio and X-rays suggest that the material is travelling and expanding at relativistic speeds. This would make the estimated mechanical power and X-ray luminosity of the jet increase by a further large factor. We hence favour the synchrotron emission mechanism for the AU-scale jet.

7.2. Conical Synchrotron Jet

A jet model with minimum free parameters is discussed in Falcke & Biermann (1999). Considering the coupled disk-jet system, subject to the assumption of total equipartition of energy between disk, jet kinetic energy, jet internal energy (thermal energy of proton/electron plasma) and magnetic field, expanding freely into vacuum, they derive a relativistic jet of terminal $\beta \sim 0.96$. (A higher velocity would require acceleration by a mechanism other than pressure gradient.) The only free parameter is the measured disk X-ray luminosity. In the case of GRS 1915+105, with X-ray luminosity of $10^{39} \text{ erg s}^{-1}$, (0.3 to 3 times this have been observed) the following properties are expected for the jet at 2 cm. The mechanical power of the jet is of the order of $Q_{\text{jet}}=10^{39} \text{ erg s}^{-1}$, which indicates a

mass accretion rate of 10^{19} g s^{-1} , assuming a conversion efficiency of 10% from gravitational energy. Note that this model assumes a maximally efficient radio jet for a given disk luminosity, i.e. a radio-loud jet. This implies, as pointed out in Falcke & Biermann (1999), that $10^{39} \text{ erg s}^{-1}$ is a **lower limit** to the mechanical power of the jet. The model then predicts a (steady state) flux density of about 20 mJy, and jet length of about 0.4 mas, with expected wavelength dependence of jet size $\Theta \propto \nu^{-1}$, and spectrum $S_\nu \propto \nu^{0.2}$. Other derived parameters are a magnetic field B of 0.4 gauss at 10 AU from the black hole, and an electron Lorentz factor γ_e in the range of 200-800.

Thus, in the steady state, the model yields roughly the correct size, spectrum, and flux of the AU-scale nuclear jet. Time variable jet length and flux density, can perhaps be accommodated as changes in mass accretion rate. Allowing for the complex time-variability in this system, we judge the agreement with our observations to be satisfactory. Next, given that the jet is already maximally radio loud, it seems to us necessary to invoke an additional mechanism, to explain the transient release of excess synchrotron emission in the flares, with spectrum $S_\nu \propto \nu^{-0.6}$. The dependence of flux density on orientation, (as in AGN unification schemes), does not apply here since we observe the axis position angle does not change sufficiently from small to large scales.

7.3. Disk Instability as the Source of Relativistic Plasma

GRS 1915+105 shows extremely complex behavior in X-rays, see e.g. Fig. 10, and Markwardt et al. (1999). The X-ray variability is explained by (Belloni et al. 1997a), and (Belloni et al. 1997b), in terms of the evacuation and refilling of the inner hot accretion disk due to thermal-viscous instability. They attempt to reduce the complexity of the light curve to essentially one parameter, the radius of the missing inner disk. The light curve, and hardness ratio variations, are decomposed into a superposition of an inner, 2.2 keV

disk component, of variable radius ($\sim 20\text{-}100$ km), along with an outer constant disk of radius over 300 km and temperature 0.5 keV. The instability (emptying/refilling of the disk) occurs in the region where radiation pressure dominates the gas pressure. The time required to refill the disk with X-ray emitting gas is set by the viscous/thermal timescale. Assuming a viscosity parameter $\alpha \sim 0.01$, they estimate this timescale as

$$t_{\text{viscous}} = 3\alpha^{-1} \left(\frac{M_{\text{BH}}}{10 M_{\odot}} \right) \left(\frac{R}{10^7 \text{cm}} \right)^{7/2} \left(\frac{\dot{M}}{10^{18} \text{g s}^{-1}} \right)^{-2} \text{ seconds} \quad (3)$$

For the 30 min dips in the X-rays (the timescale of the radio oscillations) the radius of the missing disk is of the order of 180 km. From spectral fitting to the disk/black body, they also derive a mass accretion rate of $\sim 10^{18}$ to $\sim 10^{20} \text{g s}^{-1}$, depending on whether the black hole is maximally rotating or not. The highest accretion rates are inversely correlated with the X-ray luminosity, which they take as evidence that the majority of the mass may be eliminated from view by an ADAF-type flow into the black hole.

From our AU-scale images, we find good agreement between the mass of synchrotron-emitting plasma in the AU-scale ‘mini-jet’, and the mass loss from the missing radius of the inner accretion disk. The timescales and radio/soft X-ray correlations are consistent with the disk instability model. In contrast, the large flares eject an order of magnitude more mass, and the recovery timescale of ~ 18 hrs indicates a radius of ~ 600 km for the missing disk. This is so large as to lie outside the radiation- pressure dominated region, so the instability (oscillation) would not work. Indeed, the large-scale events never repeat, unlike the AU-scale 30 min cycles. Once again, we take this as evidence of a qualitative difference between the AU-scale emission and the extreme ejections during flares. Thus the Belloni model works for mini-jets, but not for large flares.

8. Conclusions

From VLBA images of GRS 1915+105 in 1997 and 1998 we conclude the following:

1. The core is always resolved as a compact collimated jet of $\sim 10\lambda_{\text{cm}}$ AU, that has a peak brightness temperature $T_{\text{B}} \geq 10^9 \text{K}$.
2. The compact jet is observed in the **plateau** state that can last from days up to several months, which consists of a steady flat spectrum at radio wavelengths, persistently bright hard X-ray (20-100 keV) flux, and a faint flux in the softer X-rays (2-12 keV) (see Figs. 1 & 2 and Figs. 4 & 5).
3. The compact jet is observed a few hours before and a few hours after major flare/ejection events (Figs. 2 & 5). The nuclear jet is re-established in ≤ 18 hours after a major outburst. In minor outbursts the jet flux varies in ~ 30 min (Figs. 9 & 10), with the same period seen in the infrared and in the 2-12 KeV X-rays, (e.g. Mirabel et al. 1998; Fender et al. 1998; Eikenberry et al. 1998).
4. Although we could not measure the proper motion of matter in the quasi-steady compact jet, its length of ~ 20 AU (e.g. Fig. 5D & E) is comparable to the distance that would be traversed at relativistic speed during the time-scale of the oscillations (~ 30 min).
5. The compact jet is optically thick synchrotron emission. This is suggested by the high degree of collimation, the high brightness temperature, the flat radio spectrum, and the inferred relativistic bulk motions. The mass outflow assuming a synchrotron jet is $\geq 10^{-8} M_{\odot} \text{ yr}^{-1}$, consistent with the accretion rate estimated from the X-ray luminosity of the black hole binary. Thermal processes alone cannot account for the radio emission because they are relatively inefficient radiative mechanisms that would require an accretion rate **greater** than $10^{-5} M_{\odot} \text{ yr}^{-1}$, which is unreasonably large.

6. The large mass ejection events with measured superluminal velocities take place at the time of abrupt changes in the X-ray state of the source. Within $\pm 5^\circ$ the same position angles were observed for major ejections in 1994-1996 (Rodríguez & Mirabel 1999), and 1997-1998 (this paper). The change from radio-quiet to radio-loud states cannot be caused by change in orientation, since the position angle of the ejecta does not change sufficiently from small to large scales. The axis of the ejecta at large scales (≥ 500 AU) appear to be rotated clockwise by $\leq 12^\circ$ relative to the jet axis at ≤ 100 AU, both measured at the same time. The flux variations must be intrinsic.
7. Time-lapse images allow us to detect the motions of the large-scale ejecta within a few hours, with apparent speeds of ≥ 1.3 c, consistent with previous observations (Mirabel & Rodríguez, 1999). Knowing the time for the onset of the radio outburst, it is inferred that the acceleration to terminal speeds must take place within 500 AU of the black hole.
8. By astrometry over two years relative to an extragalactic reference, we locate the black hole binary within ~ 1.5 mas, and follow its secular parallax due to Galactic rotation. The black hole is stationary on the sky to ≤ 100 km s $^{-1}$, once the secular parallax is accounted for.
9. Some accreting black holes of stellar mass (e.g. Cyg X-1, 1E 1740-2942, GRS 1758-258, GX 339-4) and the supermassive black hole Sgr A*, show compact radio cores with a steady flat-spectrum plateau state, in common with the core of GRS 1915+105. It is possible that high resolution images of the other systems will also reveal compact jets. So far GRS 1915+105 is the only galactic source where both, AU-sized jets and large-scale superluminal jets have been unambiguously observed.

We thank the ASM/RXTE team for providing us with quick-look results. LFR acknowledges support from CONACyT, México. IFM acknowledges support from CONICET, Argentina.

REFERENCES

- Belloni, T., Mendez, M., King, A. R., van der Klis, M., & Van Paradijs, J. 1997, *ApJ*, 488, L109
- Belloni, T., Mendez, M., King, A. R., van der Klis, M., & van Paradijs, J. 1997, *ApJ*, 479, L145
- Blandford, R. D. & Begelman, M. C. 1999, *MNRAS*, 303, L1
- Bodo, G., & Ghisellini, G., 1995, *ApJ*, 441, L69
- Castro-Tirado, A. J., Brandt, S., Lund, N., Lapshov, I., Sunyaev, R. A., Shlyapnikov, A. A., Guziy, S., & Pavlenko, E. P. 1994, *ApJS*, 92, 469
- Dhawan, V., Goss, W. M., & Rodríguez, L.F. 2000, *ApJ*, 540, in press.
- Eikenberry, S. S., Matthews, K., Morgan, E. H., Remillard, R. A., Nelson, R. W. 1998, *ApJ*, 494, L61
- Falcke, H. & Biermann, P. L. 1999, *A&A*, 342, 49
- Fender, R.P., Garrington, S. T., McKay, D. J., Muxlow, T. W. B., Pooley, G. G., Spencer, R. E., Stirling, A. M., & Waltman, E. B. 1999, *MNRAS*, 304, 865
- Fender, R. P., Pooley, G. G., Brocksopp, C., & Newell, S. J. 1997, *MNRAS*, 290, L65
- Fender, R.P., & Pooley, G.G. 1998, *MNRAS*, 300, 573
- Fender, R.P., & Pooley, G.G., Durouchoux, P., Tilanus, R.P.J. & Brocksopp, C. 2000, *MNRAS*, in press
- Foster, R. S., Waltman, E. B., Tavani, M., Harmon, B. A., Zhang, S. N., Paciesas, W. S., & Ghigo, F. D. 1996, *ApJ*, 467, L81

- Hjellming, R. M. & Johnston, K. J. 1988, *ApJ*, 328, 600
- Kemball, A. J., Diamond, P. J., & Mantovani, F. A., 1988, *MNRAS*, 234, 713
- Ma, C., Arias, E. F., Eubanks, T. M., Fey, A. L., Gontier, A.-M., Jacobs, C. S., Sovers, O. J., Archinal, B. A., Charlot, P., 1998, *AJ*, 116, 516
- Markwardt, C. B., Swank, J. H., & Taam, R. E. 1999, *ApJ*, 513, L37
- Martí J., Mirabel, I.F., Chaty, S. & Rodríguez 2000, *ApJ*, in press
- Mirabel, I. F., Dhawan, V., Chaty, S., Rodríguez, L. F., Martí J., Robinson, C. R., Swank, J., & Geballe, T. 1998, *A&A*, 330, L9
- Mirabel, I. F. & Rodríguez, L. F. 1994, *Nature*, 371, 46
- Mirabel, I. F. & Rodríguez, L. F. 1999, *ARA&A*, 37, 409
- Narayan, R., Kato, S., & Honma, F. 1997, *ApJ*, 476, 49
- Nayakshin, S., Rappaport, S., Melia, F. 1999, AAS HEAD meeting, 31, 2801N (*ApJ* 2000, submitted)
- Pooley, G. G. & Fender, R. P. 1997, *MNRAS*, 292, 925
- Rees, M. J. 1998, in *Black Holes and Relativistic Stars*, Wald, R. M., ed., University of Chicago Press, p. 79
- Reid, M. J., Readhead, A. C. S., Vermeulen, R. C., & Treuhaft, R. N. 1999, *ApJ*, 524, 816
- Reynolds, 1986, *ApJ*, 304, 713
- Rodríguez, L. F., Gerard, E., Mirabel, I. F., Gómez, Y., and Velázquez, A., 1995, *ApJS*, 101, 173

Rodríguez, L. F. & Mirabel, I. F. 1999, *ApJ*, 511, 398

Sams, B. J., Eckart, A., & Sunyaev, R. 1996, *Nature*, 382, 47

Taylor, J. H. & Cordes, J. M. 1993, *ApJ*, 411, 674

Walker, R. C., Dhawan, V., Romney, J. D., Kellermann, K. I. & Vermeulen, R. C., 2000,
ApJ, 530, 233

Zensus, J. A., Diamond, P.J., & Napier. P. J. 1995, *Very Long Baseline Interferometry and
the VLBA*, ASP Conf. Series, Vol.82

Fig. 1.— X-ray and Radio data for 1997 October 14 to November 08 (MJD=50735 to 50760).

Top: [red] RXTE All-Sky Monitor counts, 2-12 keV; quick-look results provided by the ASM/RXTE team; [blue] BATSE fluxes, 20-100 keV from occultation measurements, (photons $\text{cm}^{-2} \text{s}^{-1}$, multiplied by 2000 for plotting).

Middle: GBI radio flux densities at 13 and 3.6 cm.

Bottom: GBI radio spectral index. The radio data is typically ~ 10 scans per day of 5 min each, separated by 30-60 min. Note the correlation between the start of the soft X-ray and radio flares, and the similar decay times of the BATSE and radio fluxes. The VLBA observed in the periods indicated by the black V's labelled A, B, & C, with the corresponding images in Fig.2. The vertical green line is our estimate of the start of the flare at MJD=50749.8 \pm 0.1 day.

Fig. 2.— VLBA images during 1997 October, corresponding to epochs A, B, & C in Fig. 1. Contours are at -5%, 5, 10, 20, 40, 60, & 90% of peak.

(A) 2 cm image with 7.5 AU resolution, during a plateau state, showing the jet in the nucleus, 6 days before the flare in B & C; peak = 15.7 mJy beam $^{-1}$.

(B) 13 cm image with 220 AU resolution; peak = 93.7 mJy beam $^{-1}$.

(C) 3.6 cm image, with 80 AU resolution; peak = 19.7 mJy beam $^{-1}$.

B and C are simultaneous data, centered at epoch MJD=50752.02, 53.3 \pm 2.4 hours after the estimated start of the flare. The position of **A** is the same as the central component of **C** within 1.5mas. The black “*” marks the astrometric position of the nucleus, here and in Fig. 7 A, item 5.

Fig. 3.— Images at 3.6 cm, of the same data as in Fig.2C, epoch 1997 Oct 31. Contours are at -4%, 4, 8, 16, 32, 64, 96% of peak. The SE component has a proper motion of 2.3 \pm 0.2 mas

during 2.5 hrs, or 0.92 ± 0.08 mas hr^{-1} . The mean position of the SE component implies a motion of 47.5 ± 0.3 mas in 53.3 ± 2.4 hrs since the start of the flare, or 0.90 ± 0.05 mas hr^{-1} .

Fig. 4.— X-ray and radio data for 1998 April 07 to May 12 (MJD=50910 to 50945). Details are as in Fig. 1. Images from VLBA data, indicated by the black V's labelled D, E, & F, are shown in Fig. 5. The vertical green line is our estimate of the start of the flare at MJD=50932.7 \pm 0.3 days.

Fig. 5.— VLBA images during 1998 April-May, corresponding to epochs D, E, and F in Fig. 4. Contours are at -2%, 2, 4, 8, 16, 32, 64, 96% of the peak.

(D) 2 cm image, 7.5 AU resolution, showing the nuclear jet during a plateau state, 2 days before the flare on MJD 50916; peak = 48 mJy beam $^{-1}$.

(E) 2cm image, 7.5 AU resolution; peak = 64 mJy beam $^{-1}$.

(F) 0.7cm image, 2.5 AU resolution; peak = 66.4 mJy beam $^{-1}$.

E and F are quasi-simultaneous data (see Table-1), centered at MJD 50935.50. The position of **E** is identical to **D** within 1.0 mas. The black '+' marks the astrometric position, here and in Fig. 7 A, item 7.

Fig. 6.— Lower resolution images at 2 cm, of the same data as in Fig.5, epoch 1998 May 02 at 75 AU resolution. Contours are at -2%, 2, 3, 4, 6, 8, 16, 32, 64, 96% of peak. The blue and red contours show time-resolved images 4.5 hrs apart. The SE component has a proper motion of 4.2 ± 0.3 mas, or 0.93 ± 0.07 mas hr^{-1} . The mean position of the SE component implies a motion of 57.5 ± 0.5 mas in 67 ± 7 hrs since the start of the flare, or 0.87 ± 0.10 mas hr^{-1} .

Fig. 7.— A: Astrometric positions from 1996 May, to 1998 May, showing that the motion of GRS1915+105 lies mainly in the galactic plane. Key:

[1]=1996 May 23, 3.6 cm. [2]=1996 Aug 04, 3.6 cm. [3]=1997 May 15, 3.6 cm, rise. [4]=1997 May 15, 3.6 cm, set. [5]=1997 Oct 23, 2 cm, pre-flare. [6]=1997 Oct 31, 3.6 cm, during flare. [7]=1998 Apr 11, 2 cm, pre-flare. [8]=1998 May 02, 2 cm, during flare. The sloping line is parallel to the Galactic plane.

B: Expected secular parallax from galactic rotation vs. distance, in the direction of GRS1915+105, assuming 220 km s^{-1} rotation, (solid line). If the source were at 12 kpc, and stationary with respect to the galactic surroundings, 5.3 mas yr^{-1} is expected, compared to the $5.8 \pm 1.5 \text{ mas yr}^{-1}$ measured. The effect of a $\pm 10\%$ ($\pm 22 \text{ km s}^{-1}$) variation in rotation velocity is shown as the dashed lines.

Fig. 8.— Deconvolved core size (Gaussian FWHM) vs. wavelength. Galactic electron scattering is fitted to the intrinsically unresolved minor axis, (lower line) $\Theta_{\text{min}} = (0.15\lambda_{\text{cm}}^2)\text{mas}$. An intrinsically elongated source, plus scattering, is independently fit to the major axis, (upper line), $\Theta_{\text{Maj}} = (1.0\lambda_{\text{cm}} + 0.14\lambda_{\text{cm}}^2)\text{mas}$.

The solid lines are fitted to data from a single day (1996 Aug 01) when the flux from the core was steady. Dashed lines extend to newer data (1998 May 02) at 2 cm and 0.7 cm. The Y-axis at right shows the linear size at an assumed distance of 12 kpc. The jet length is variable by up to a factor of ~ 2 at different epochs.

Fig. 9.— Radio flux density variations at three wavelengths, monitored by the VLA during the plateau state on 1997 May 15, 06-16 UTC. Inset is the VLBA at 2 cm, from observations during the gap in the VLA coverage from 10-12 UTC.

Fig. 10.— Top: XTE 2-12keV counts on 1997 Sep 05, 06-10 UTC. Note the dips every ~ 12 min.

Bottom: VLA flux density at 3.6 cm, with the same periodicity (within errors) as the X-ray dips. Fig. 9 and Fig. 10 taken together, support the idea that the radio oscillations arise in a synchrotron jet of (Gaussian FWHM) size $\sim 10\lambda$ AU, which is fed by plasma injected during the dips in the soft X-ray flux.

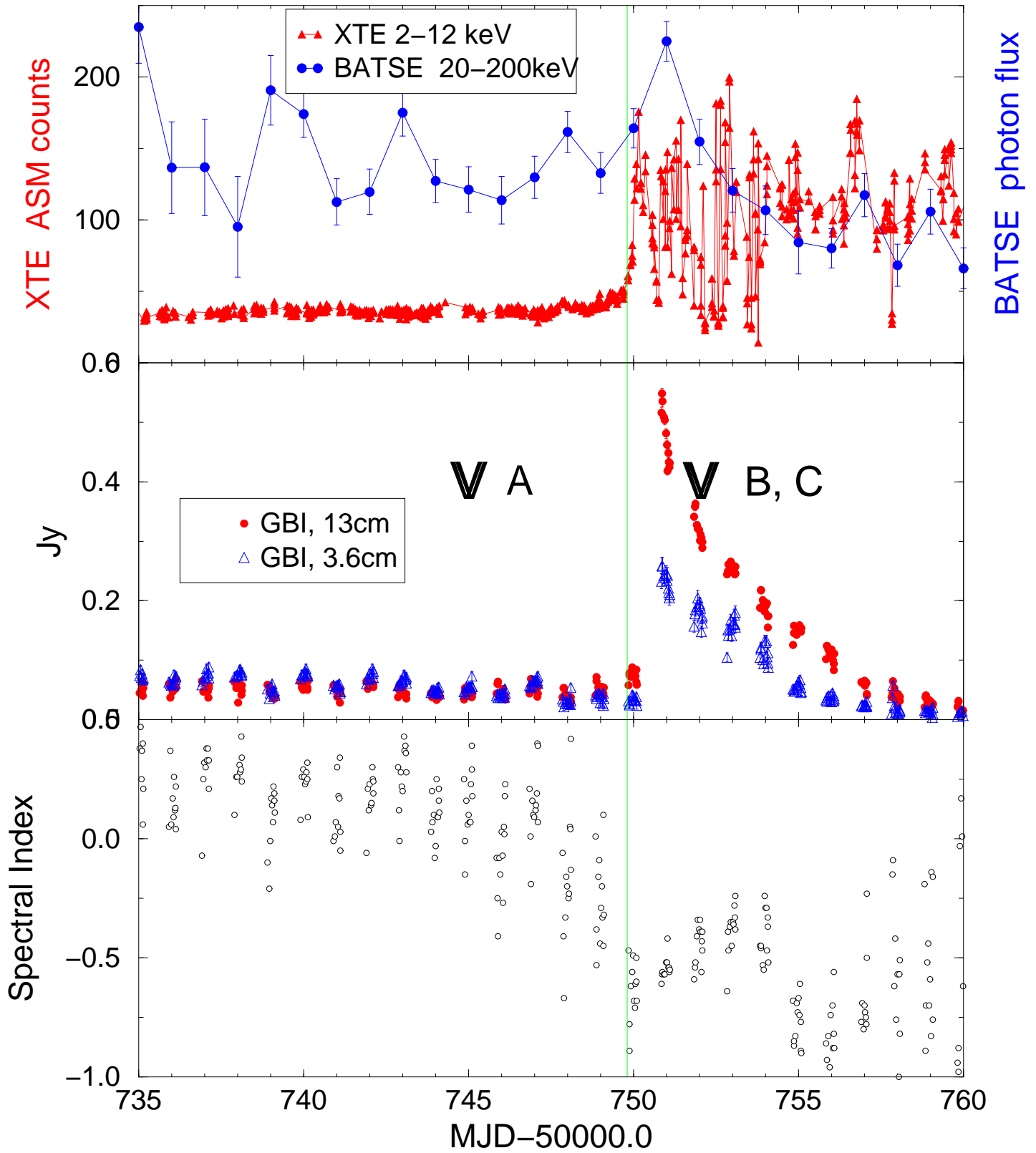
	MJD	UT	Fig.	λ (cm)	Bit rate (Mb s ⁻¹)	rms, M. (μ Jy)	rms, T. (μ Jy)	beam (mas)
A	50744	97 Oct 23 22:15-03:23	2 A	2.0	256	210	85	0.62
B	50751	97 Oct 30 23:00-04:08	2 B	13	128 ^B	180	75	20.
C	50751	97 Oct 30 23:00-04:08	2 C	3.6	128 ^C	200	75	7.0
D	50914	98 Apr 11 09:00-14:08	5 D	2.0	256	230	85	0.62
E	50935	98 May 02 07:35-15:55	5 E	2.0	128 ^E	260	120	0.62
F	50935	98 May 02 08:26-16:22	5 F	0.7	256 ^F	510	300	0.21

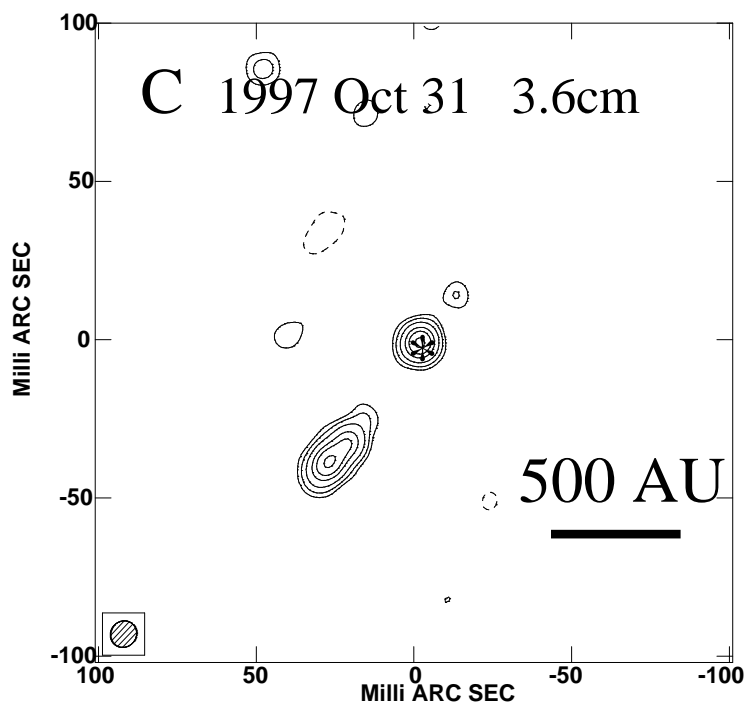
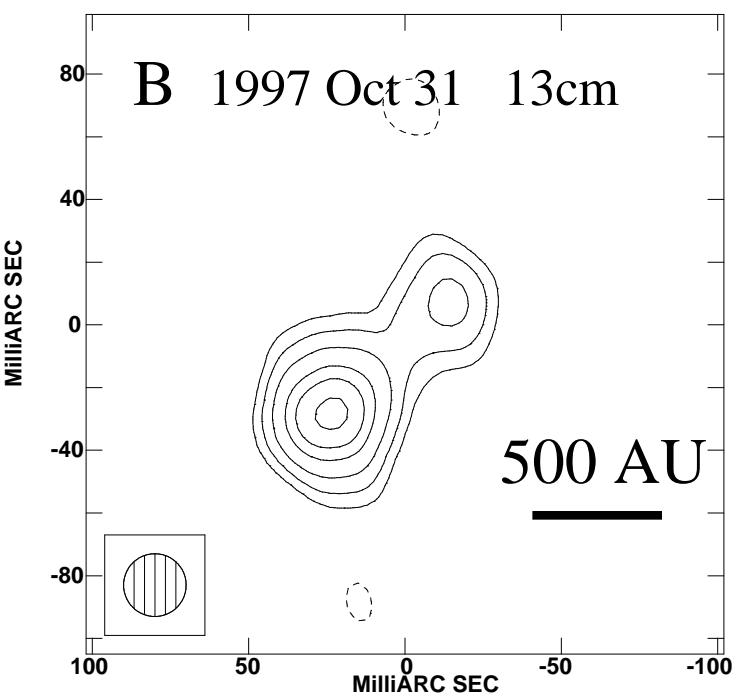
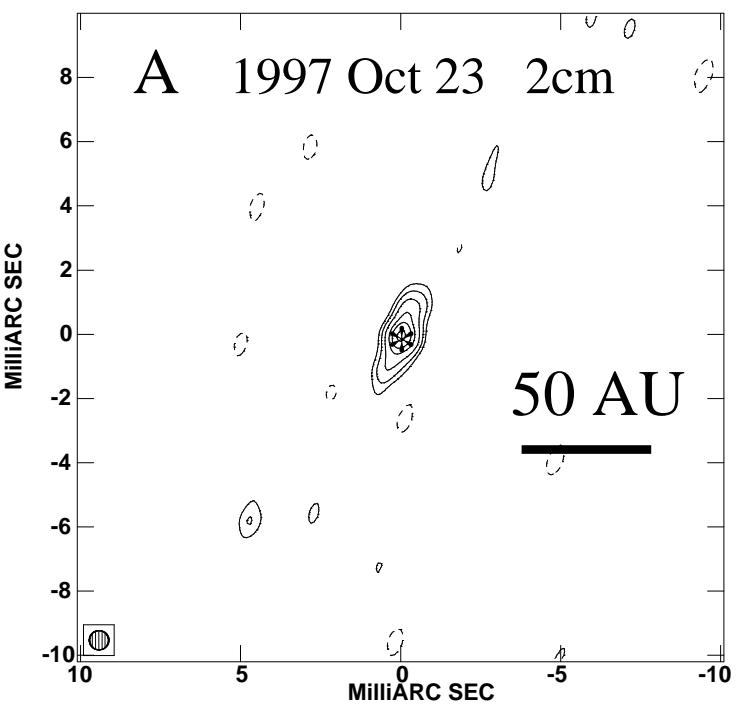
B, & C in Fig. 2 were simultaneous observations, 128 Mb/s was recorded at each of 3.6 cm and 13 cm.

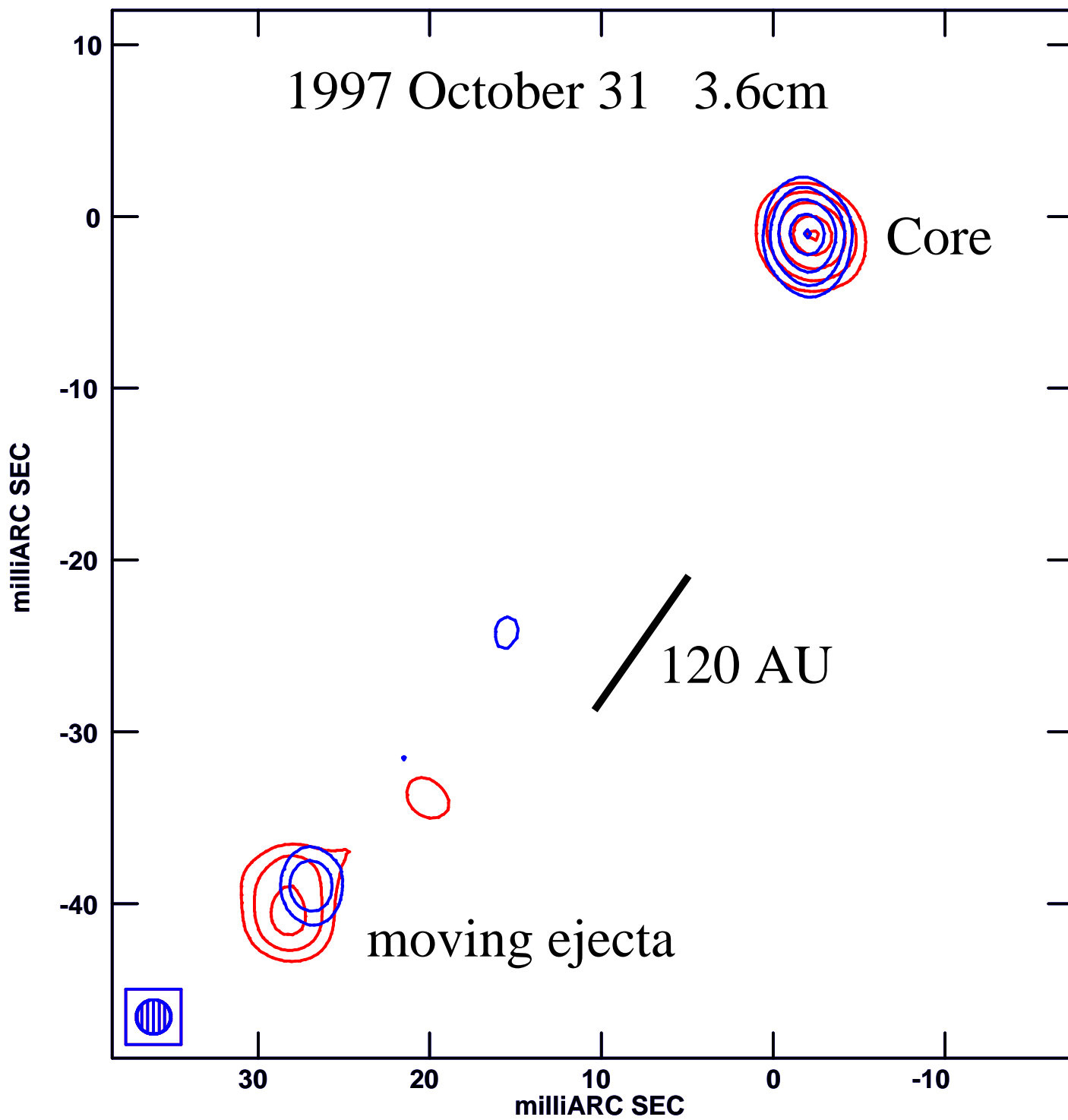
E, & F in Fig. 5 were quasi-simultaneous observations, the sequence (128 Mb/s for 44 min at 2 cm, 5 min dead time, then 256 Mb/s for 22 min at 7 mm) was repeated 7 times.

Table 1: VLBA observations. The columns are: Observation Epoch; Figure reference; Wavelength; Bit rate, megabits per second; rms noise in image, microJansky per beam area, measured; RMS noise, theoretical; and Synthesized Beam FWHM, mas.

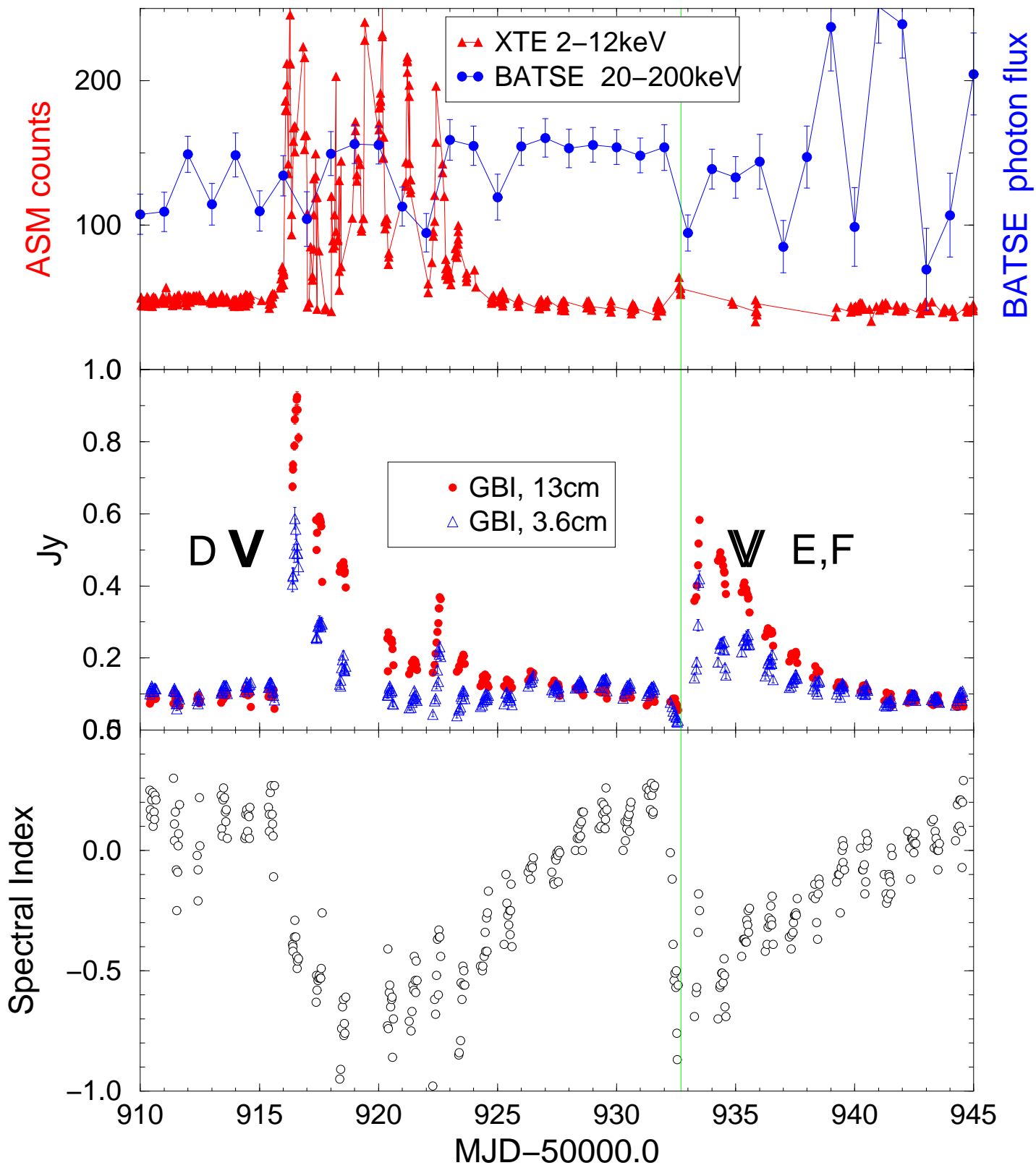
1997 October 14 – November 08

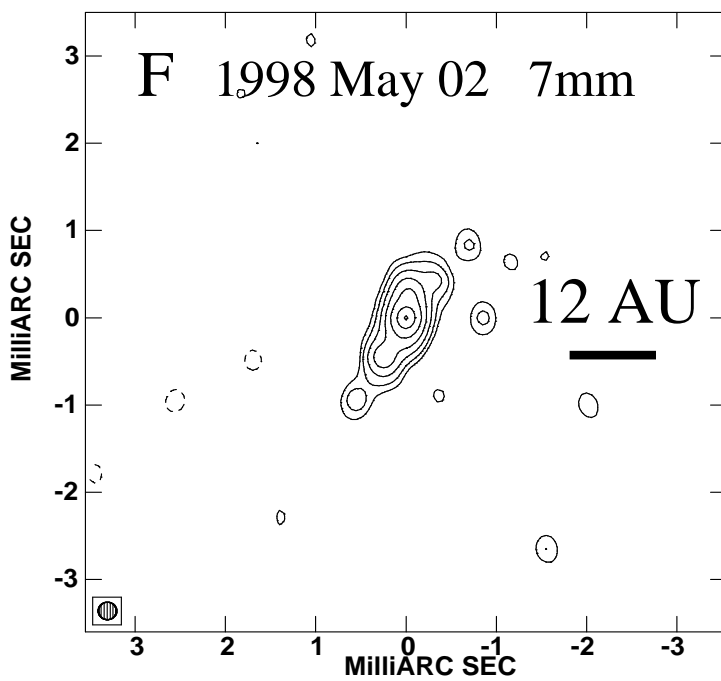
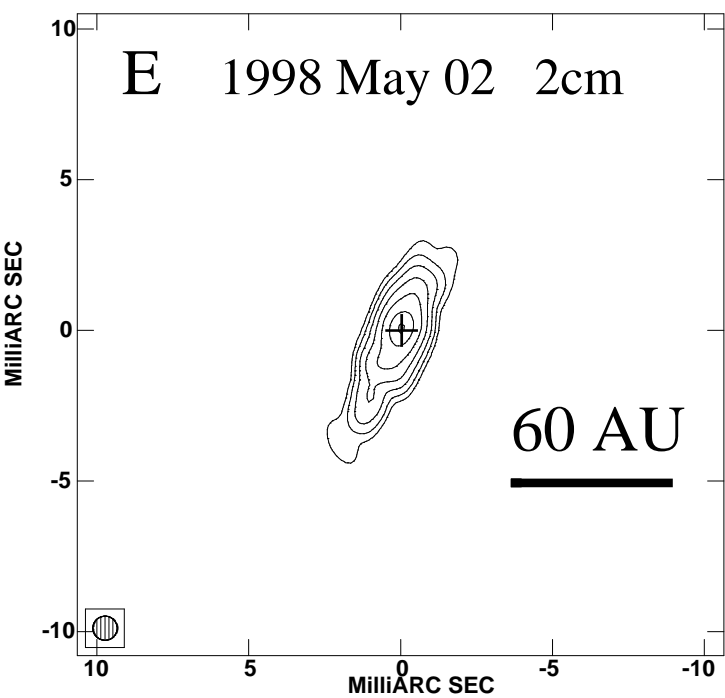
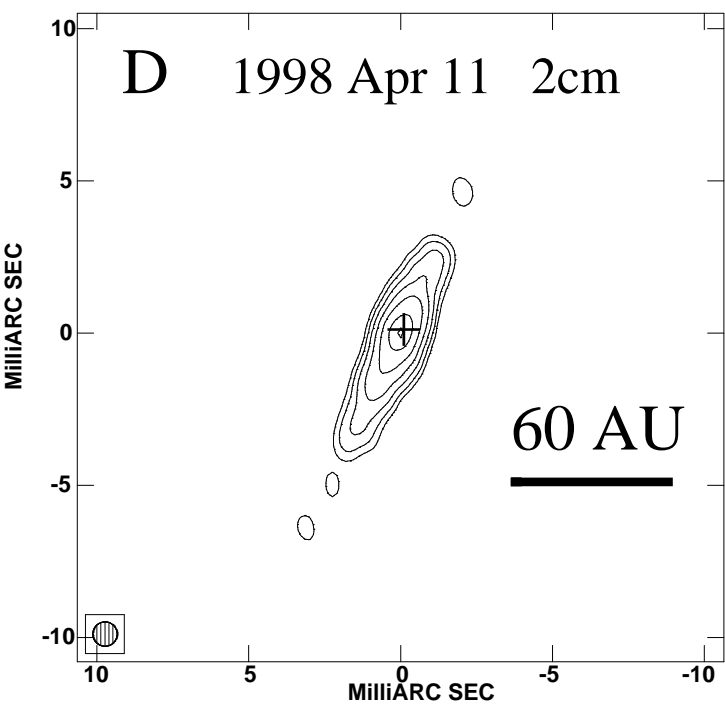


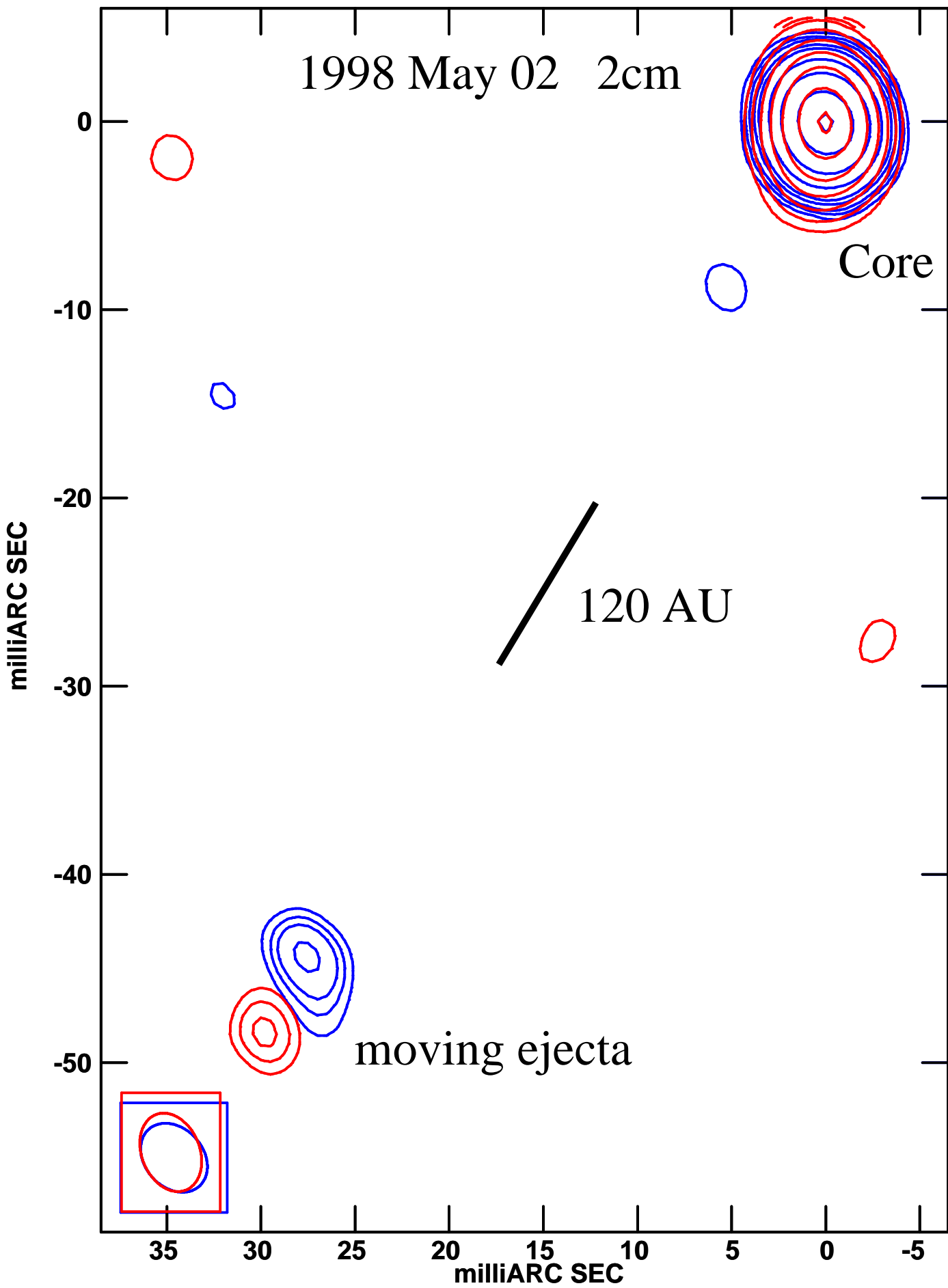




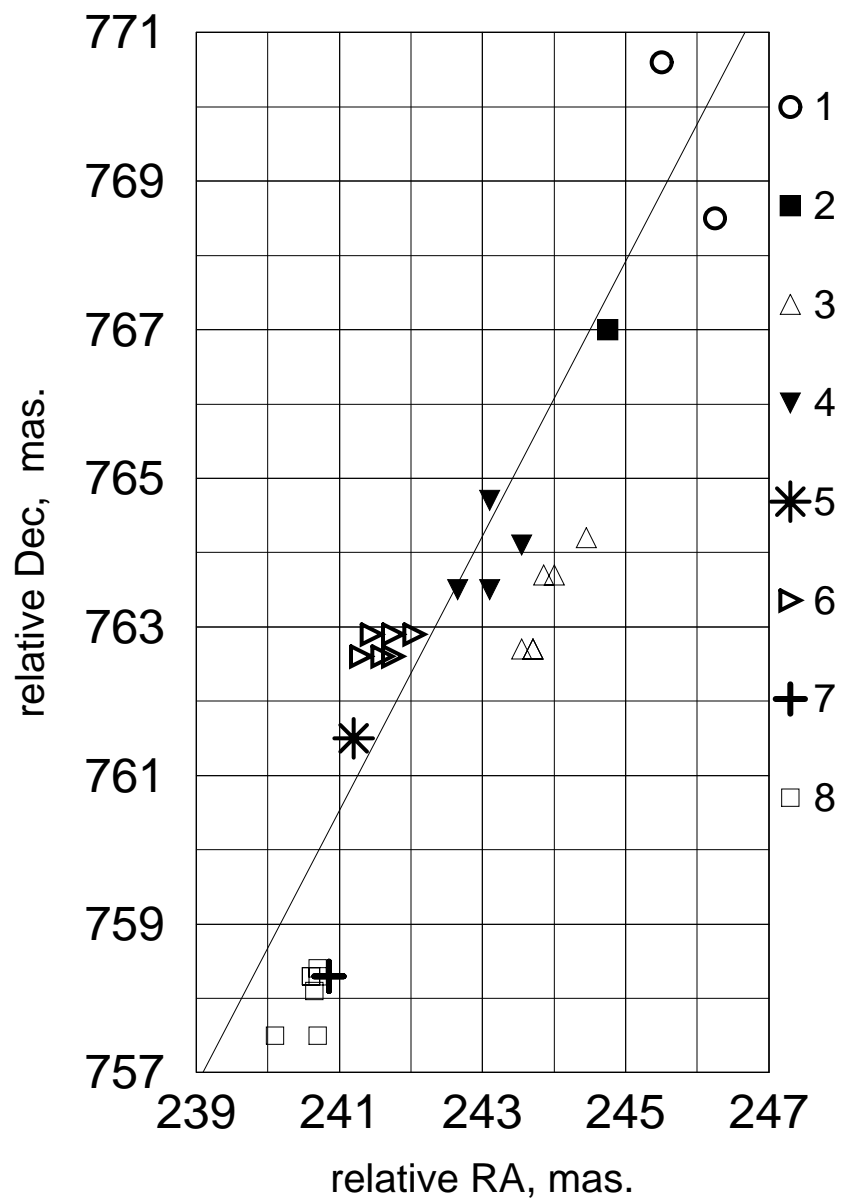
1998 April 07 – May 12



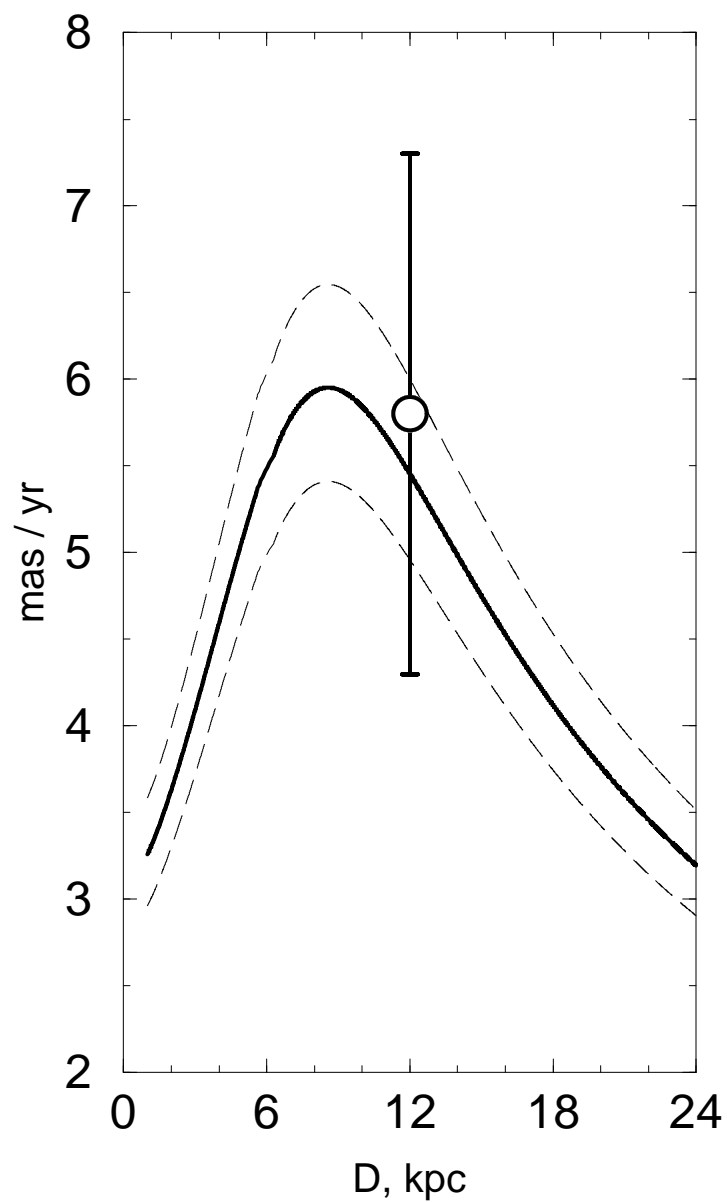




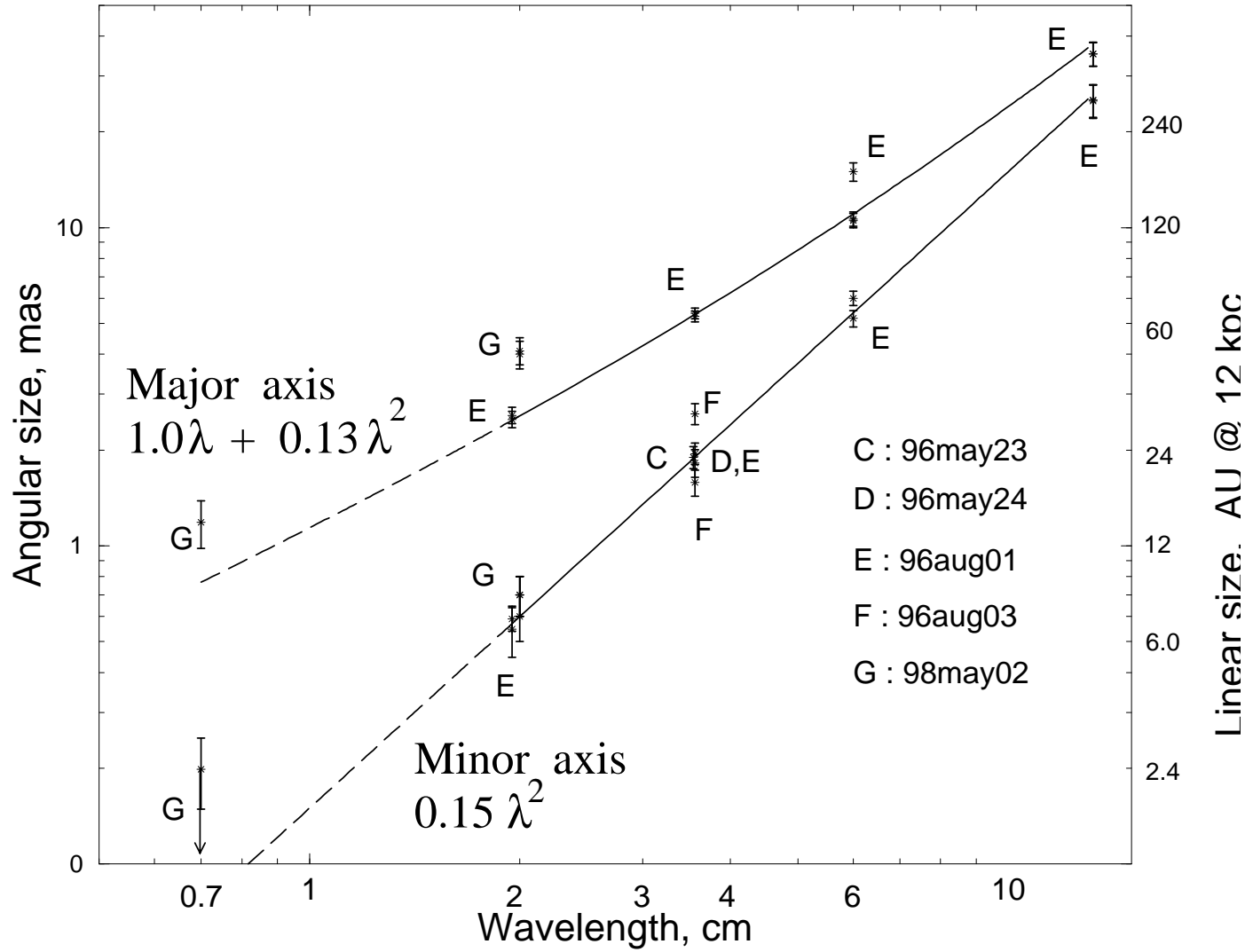
A: Core Position



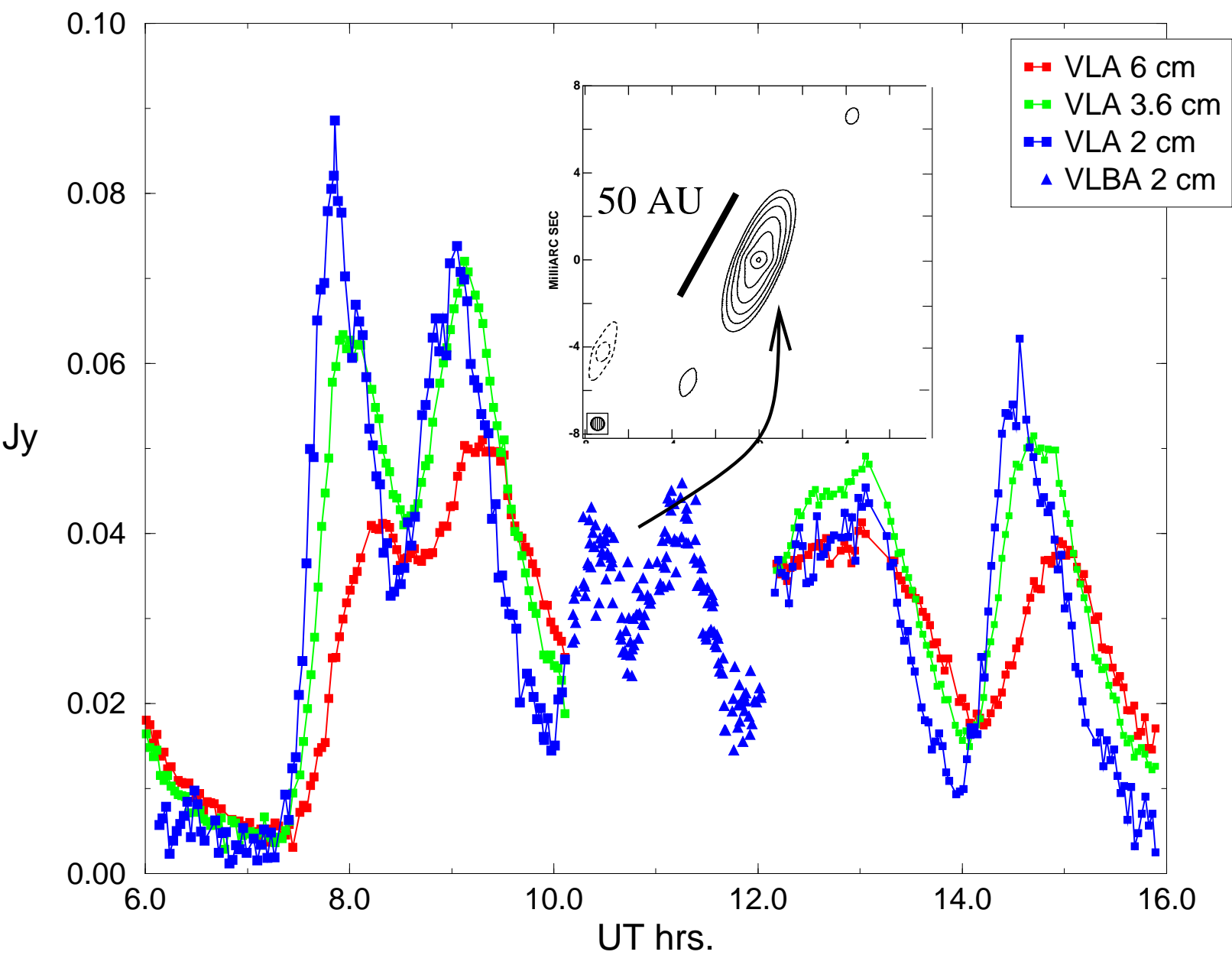
B: Secular Parallax



GRS 1915: Core size vs. Wavelength

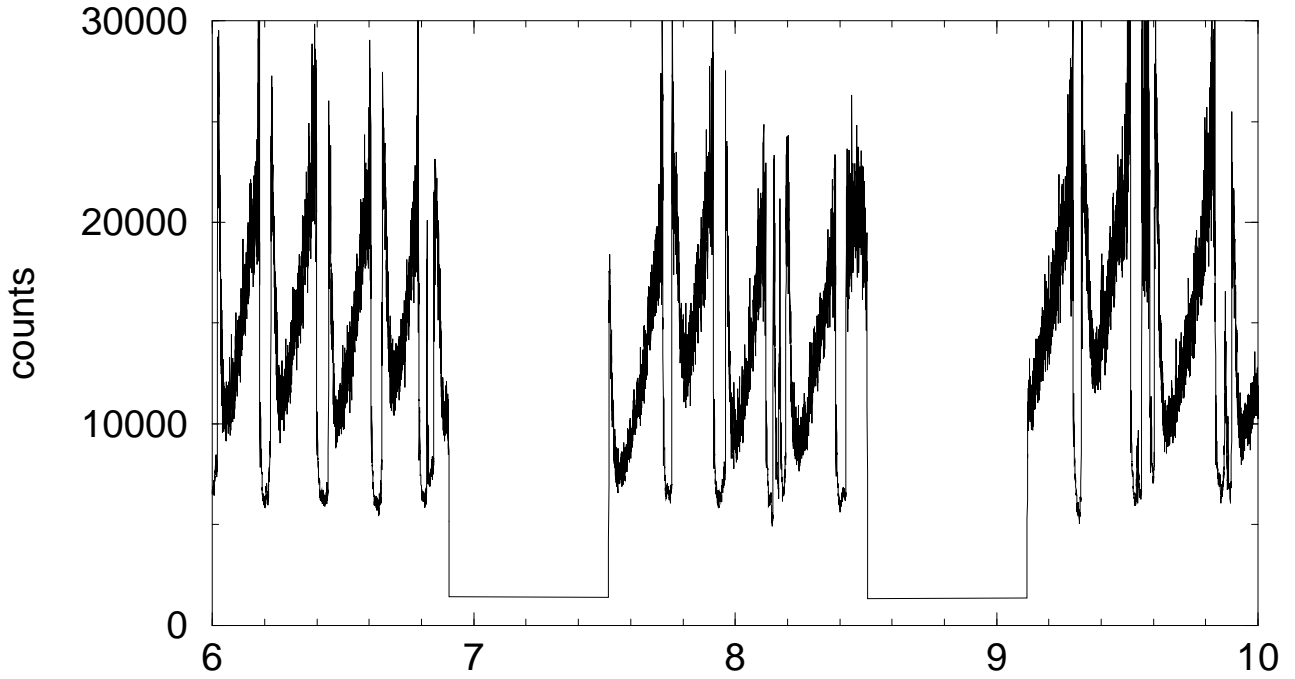


1997 May 15



1997 Sep 05

RXTE 2–12 KeV X-ray



VLA 3.6cm Radio

